



Structural, electrical and electrochemical characteristics of $\text{La}_{0.1}\text{Sr}_{0.9}\text{Co}_{1-x}\text{Nb}_x\text{O}_{3-\delta}$ as a cathode material for intermediate temperature solid oxide fuel cells

Journal:	<i>RSC Advances</i>
Manuscript ID:	RA-ART-03-2014-002061.R1
Article Type:	Paper
Date Submitted by the Author:	03-Apr-2014
Complete List of Authors:	Yoo, Seonyoung; UNIST, School of Energy and Chemical Engineering Kim, Jiyoun; Agency for Defense Development, Convergence Technology Research Directorate Lee, Dong Woo; Chung-Ang University, Chemistry Song, Seung yoon; Chung-ang univ., Shin, Jeeyoung; Dong-Eui University, Dept. of Mechanical Eng. Ok, Kang Min; Chung-Ang University, Chemistry Kim, Guntae; UNIST, School of Energy and Chemical Engineering

Structural, electrical and electrochemical characteristics of $\text{La}_{0.1}\text{Sr}_{0.9}\text{Co}_{1-x}\text{Nb}_x\text{O}_{3-\delta}$ as a cathode material for intermediate temperature solid oxide fuel cells

Seonyoung Yoo^a, Jiyoun Kim^b, Seung Yoon Song^c, Dong Woo Lee^c, Jeeyoung Shin^d, Kang Min Ok^{*c}, Guntae Kim^{*a}

^a*School of Energy and Chemical Engineering, Ulsan National Institute of Science and Technology (UNIST), Ulsan, 689-798, Republic of Korea*

^b*Convergence Technology Research Directorate, Agency for Defense Development, Daejeon, 305-600, Republic of Korea*

^c*Department of Chemistry, Chung-Ang University, Seoul 156-756, Republic of Korea*

^d*Department of Mechanical Engineering, Dong-Eui University, Busan 614-714, Republic of Korea*

The perovskite-oxides, such as $(\text{La,Sr})\text{CoO}_3$, have received a large amount of attention in recent years as cathode materials for intermediate temperature-solid oxide fuel cells (IT-SOFCs). In this study, we have investigated the structural, electrical, and electrochemical properties of $\text{La}_{0.1}\text{Sr}_{0.9}\text{Co}_{1-x}\text{Nb}_x\text{O}_{3-\delta}$ ($x = 0, 0.1, 0.15, \text{ and } 0.2$) cathodes under IT-SOFC operating conditions. Nb doping significantly improves the structural stability and electrochemical performance of $\text{La}_{0.1}\text{Sr}_{0.9}\text{Co}_{1-x}\text{Nb}_x\text{O}_{3-\delta}$ (LSCNbx) oxides compared to undoped $\text{La}_{0.1}\text{Sr}_{0.9}\text{CoO}_{3-\delta}$ (LSC). At a given temperature, the electrical conductivity decreases with further increases of the Nb doping content. The electrochemical performance of LSCNbx-GDC cathodes is measured using LSCNbx-GDC/GDC/Ni-GDC anode supported cell. For LSCNbx ($x = 0.1$), the maximum power density of a single cell is 1.478 W cm^{-2} at $600 \text{ }^\circ\text{C}$. The Nb doped LSCNbx ($x = 0.1$) perovskite is recommended, considering its high power density and structural stability as an IT-SOFC cathode material.

Keyword: Cathode; Electrochemical performance; Perovskite; Solid oxide fuel cells; Structural stability

** Corresponding authors: kmok@cau.ac.kr, gtkim@unist.ac.kr; Fax: +82 52 217 2909*

Introduction

One of the most promising energy conversion devices, solid oxide fuel cells has recently received a great deal of attention because of their high efficiency, low pollutant, and fuel flexibility, etc. The requirement for high operating temperature (800-1000 °C) of conventional SOFCs, however, leads to notable problems such as high costs and high rate of degradation due to the interactions between cell components during cell fabrication and/or operation. To overcome these problems, researchers have strived to lower the SOFC operating temperature toward an intermediate-temperature (IT) range (500-700 °C). One of the challenges for IT-SOFCs, however, is to develop cathode materials with sufficiently high electrocatalytic activity for oxygen reduction.¹⁻⁶

A preferable cathode material for IT-SOFCs should have high electronic and oxide ion conductivities, and high catalytic activity for the oxygen reduction reaction. In this regard, mixed ionic and electronic conductors (MIECs) containing Mn, Fe, Co, and/or Ni with the capability to conduct oxygen ions and electrons simultaneously are strong candidates as IT-SOFC cathodes.⁷⁻¹² Among those various MIEC oxides, perovskite systems continue to dominate the research on SOFC cathodes, and there has been increasing interest in Co-containing systems in particular due to their high electronic and oxide ion conductivity.⁸⁻¹¹

Among Co-containing perovskite materials, lanthanum-doped strontium cobaltites ((La,Sr)CoO_{3-δ}) have been studied extensively due to the favorable electrical properties.^{1,12} The high catalytic activity of LSC was meanwhile explained by its high ionic conductivity with lower overpotential and high oxygen vacancy concentration, which facilitates rapid migration of oxygen species through the bulk as well as the surface of the electrode material. The oxygen vacancies located in the lattice of a cathode material are an important factor to determine the

oxygen reduction process as well as the electronic conduction. Oxygen vacancies are not only carriers for oxide ion transport through the cathode but also active sites for oxygen adsorption, dissociation, and diffusion. Both high oxygen vacancy concentration and high electronic conductivity would be beneficial for reducing the resistance of the oxygen reduction reaction (ORR).^{1,13,14}

However, one of the problems with (La,Sr)CoO_{3-δ} perovskite cobaltites is the stability of competing hexagonal phases at high cobalt oxidation states (> +3). These hexagonal phases can influence degradation over time and impair their performance as SOFC cathodes.¹² Another problem is the ordering of oxygen vacancies that has been demonstrated to occur in (La,Sr)CoO_{3-δ} below 750 °C at $p(\text{O}_2)$ below 0.1 atm. These problems give rise to a significant decrease in electronic and ionic conductivity, in addition to mechanical instability associated with lattice expansion.^{12,15-17}

This incompatibility can cause structural instability of cathode materials in operating SOFCs and thus result in poor long-term thermal stability. Therefore, to enhance the structural stability of LSC-based perovskites, one strategy is to dope their B-sites via suitable cations. Nagai *et al.* demonstrated that the stability of the perovskite structure is enhanced by substituting B-sites with cations having a higher valence and Nb is the most effective dopant for improving the chemical stability of Co-based perovskite oxides.^{18,19} It has been reported that the introduction of Nb in the B-sites of cobalt-based perovskites can improve the electrochemical performance and chemical stability for SOFC application, with 10% Nb doping on BaCo_{1-x}Fe_xO_{3-δ}.^{20,21}

The aim of this study is to present the structural-stabilization effect of Nb doping in the B-site of the perovskite La_{0.1}Sr_{0.9}Co_{1-x}Nb_xO_{3-δ} (LSCNbx), which shows considerably good structural stability and high electrochemical performance. The behavior of Nb doped LSC is illustrated

through the structural, electrical, and electrochemical characterization in terms of its application as a cathode for IT-SOFCs.

Experimental

LSCNbx ($x = 0, 0.1, 0.15, \text{ and } 0.2$) phases were synthesized through standard solid-state reaction techniques. La_2O_3 was dried overnight at $1000\text{ }^\circ\text{C}$ before being used. Stoichiometric amounts of La_2O_3 (Waco, 99.99%), SrCO_3 (Aldrich, 99.9%), Co_2O_3 (Junsei, 99%), and Nb_2O_5 (Fluka, 99.9%) were thoroughly mixed with an agate mortar and pestle and pressed into pellets. The pellets in alumina boats were gradually heated to $1200\text{ }^\circ\text{C}$ for 24 h with an intermediate regrinding. All the samples were cooled, reground, and repelletized during the intermediate heating. The samples were cooled at a rate of $5\text{ }^\circ\text{C h}^{-1}$ to room temperature.

The X-ray powder diffraction data were collected on a Bruker D8-Advance diffractometer using $\text{Cu K}\alpha$ radiation at room temperature with 40 kV and 40 mA. The 2θ range was $10\text{--}110^\circ$ with a step size of 0.02° , and a step time of 1 s. High-temperature XRD studies were carried out in air ranging from $100\text{ to }800\text{ }^\circ\text{C}$ (Bruker D8 Advance, $\text{Cu K}\alpha$ radiation) with measurements made every $100\text{ }^\circ\text{C}$. The diffraction patterns were analyzed using the Rietveld method with the GSAS program.²² The structural refinement of the materials was carried out in the space group $Pm\text{-}3m$ (No. 221) with a starting model based on the reported data of $\text{La}_{0.1}\text{Sr}_{0.9}\text{CoO}_3$.²³ A total of 25 parameters were used during the refinements. An asymmetry correction was applied to the low-angle reflections. The scale was initially refined, followed in subsequent iterations by the zero point error, unit-cell, peak shape, and overall isotropic displacement parameters. No crystallographic ordering between Co^{3+} and Nb^{5+} cations was observed. In the solid solutions of LSCNbx ($x = 0.1, 0.15, \text{ and } 0.2$), the Co^{3+} and Nb^{5+} were statistically disordered over the

transition metal sites. The resulting formulas are in good agreement with the reported stoichiometry. The results of the crystallographic data and selected bond distances (Å) for LSCNbx ($x = 0.1, 0.15, \text{ and } 0.2$) solid solutions are summarized in Table 1 and 2, respectively.

The microstructures and morphologies of LSCNbx cathode samples were observed using a field emission scanning electron microscope (SEM) (Nova SEM). A thermogravimetric analysis (TGA) was carried out using a SDT-Q600 (TA instrument, USA). TGA experiments were performed from 100 °C to 900 °C with a heating/cooling rate of 2 °C min⁻¹ in air. The room-temperature oxygen content values were determined by iodometric titration.

Symmetrical electrochemical cells with a configuration of electrode/GDC/electrode were applied for the impedance studies. Ce_{0.9}Gd_{0.1}O_{1.95} (GDC) was used for the electrolyte to avoid interfacial reactions between the electrolyte and the cathode, because the LaGaO₃ based electrolyte (LSGM) and yttria-stabilized zirconia electrolyte (YSZ) may react with the La-doped strontium cobaltites.²⁴ The GDC powder was pressed into pellets, and sintered at 1350 °C for 4 h in air to obtain a dense electrolyte substrate. The cathode slurry was painted onto both surfaces of the dense GDC electrolyte symmetrically and subsequently sintered at 950 °C for 4 h under an air atmosphere.

Electrochemical performance of the LSCNbx ($x = 0.1, 0.15, \text{ and } 0.2$) cathode was evaluated with Ni-GDC anode-supported single cells. To measure cell performance, LSCNbx ($x = 0.1, 0.15, \text{ and } 0.2$) powders and GDC were mixed at a weight ratio of 6 : 4 and ball-milled for 12 h. The Ni-GDC cermet anode, thereafter, was fabricated from a mixture of nickel oxide, GDC prepared by GNP, and starch at a weight ratio of 6 : 4 : 1.5. This mixture was ball-milled in ethanol for 24 h. The GDC powder electrolyte was pressed over the pelletized Ni-GDC cermet anode. The Ni-GDC/GDC anode-electrolyte layer was sintered at 1350 °C for 5 h. For the top layer cathode,

LSCNbx ($x = 0.1, 0.15, \text{ and } 0.2$) slurries were painted on the GDC electrolyte. The cells, with an active electrode area of 0.36 cm^2 , were finally sintered at $950 \text{ }^\circ\text{C}$ for 4 h under an air atmosphere. Ag wires were attached to both the anode and cathode of a single cell using Ag paste (SPI Supplies, 05063-AB) as a current collector. An alumina tube was employed to fix the single cell using a ceramic adhesive (Aremco, Ceramabond 552). H_2 containing 3 % H_2O was applied through a water bubbler with a flow rate of 20 mL min^{-1} , while air was applied as an oxidant and supplied to the cathode by ambient air flow during the single cell test. A BioLogic Potentiostat was used to measure impedance spectra and I - V curves. Impedance spectra were recorded under OCV in a frequency range of 1 mHz to 500 kHz with AC perturbation of 14 mA at $700 \text{ }^\circ\text{C}$. I - V polarization curves were measured between 500 to $650 \text{ }^\circ\text{C}$.

Results and Discussion

LSCNbx ($x = 0, 0.1, 0.15, \text{ and } 0.2$) exhibits a perovskite structure crystallizing in a centrosymmetric cubic space group $Pm-3m$ (No. 221) (see the ESI). The B-site is occupied by Co^{3+} or Nb^{5+} and the cations are bonded to six oxygen atoms in a regular octahedral environment with bond length ranging from $1.92107(10)$ to $1.93752(2) \text{ \AA}$ depending on x . In the A-site, Sr^{2+} or La^{3+} cations are present with A–O contact distances ranging from $2.71680(10)$ to $2.74007(2) \text{ \AA}$. For comparison, lists of the selected bond distances for LSCNbx ($x = 0, 0.1, 0.15, \text{ and } 0.2$) are given in Table 2. The bond distances are consistent with those previously reported.^{2,25}

We were able to substitute up to 20 % of Nb^{5+} cations for Co^{3+} to form solid solutions, *i.e.*, LSCNbx ($x = 0.1, 0.15, \text{ and } 0.2$). The powder X-ray diffraction data for solid solutions of $\text{La}_{0.1}\text{Sr}_{0.9}\text{Co}_{1-x}\text{Nb}_x\text{O}_3$ are shown in Fig. 1 with the refined parameters given in Table 1. As can be seen clearly from the powder X-ray diffraction patterns in Fig. 1, the peak positions shift to the

left-hand side and the peak widths broaden as the amount of doped Nb^{5+} increases. As expected, the cell volume increases with increasing Nb^{5+} on the Co^{3+} site, which is attributed to the larger size of Nb^{5+} compared with the relatively smaller size of Co^{3+} . While the ionic radius of six-coordinate Nb^{5+} is known to be 0.64 Å, that for six-coordinate Co^{3+} is known to be smaller, 0.61 Å.²⁶ Thus, the unit-cell parameters and the cell volumes increase with increasing Nb^{5+} on the Co^{3+} site (see Fig. 2). The peak broadening may be attributable to the increased statistical disordering between Co^{3+} and Nb^{5+} cations. We did not observe any ordering between Nb^{5+} and Co^{3+} in the LSCNbx phase. The experimental, calculated, and difference diffraction plots for LSCNbx ($x = 0.1$) are also shown in Fig. 3.

To check the structural stability of LSCNbx ($x = 0, 0.1$), XRD measurements were carried out after annealing at 800 °C for 350 h. As seen in Fig. 4, the XRD results show that LSCNbx ($x = 0$) structurally changes from cubic to hexagonal, while LSCNbx ($x = 0.1$) maintains a cubic perovskite structure. This indicates that the cubic perovskite phase is efficiently stabilized after annealing at high temperature, when the LSCNbx oxides are doped with Nb for Co at $x = 0.1$.

In order to confirm the phase stability at various temperatures (100 to 800 °C) in air, high-temperature XRD measurement was carried out and the results are presented in Fig. 5(a). The in-situ XRD patterns of the LSCNbx ($x = 0.1$) at various temperatures showed that the material retained its perovskite structure over the temperature range (100 to 800 °C). As shown in Fig. 5(b), with increasing temperature, the main diffraction peaks obviously shift to lower 2θ , indicating that the volume of the unit cell increases.

The thermogravimetric analyses diagrams of LSCNbx ($x = 0.1, 0.15, \text{ and } 0.2$) with temperature in air are shown in Fig. 6. The room temperature oxygen contents of LSCNb_{0.1}, LSCNb_{0.15}, and LSCNb_{0.2} are set to be 2.745, 2.715, and 2.720, respectively, through

iodometric titrations. The TGA curves show that significant weight losses occur above 350 °C due to the loss of oxygen from the lattice. The total weight loss of the sample over the entire temperature range decreases with increasing Nb content, possibly due to the stronger Nb-O bond compared to the Co-O bond, which would suppress the oxygen loss of the samples with high Nb content upon heating the samples.²⁷

The temperature dependence of the electrical conductivity of LSCNbx ($x = 0.1, 0.15, \text{ and } 0.2$) in air is presented in Fig. 7. The electrical conductivity decreases with higher Nb content mainly due to decreasing $\text{Co}^{3+/4+}$ which is consistent with previous results.²⁸ For $x = 0.1$, the faster decrease in conductivity at higher temperatures could be due to the formation of a significant amount of oxide ion vacancies.^{1,2} As shown in Fig. 7, the electrical conductivity decreases with the Nb doping content. A different trend has been observed in LSCNbx ($x = 0.1, 0.15, 0.2$) electrical conductivity results. LSCNbx ($x = 0.1$) samples presents different slope of electrical conductivity compared to LSCNbx ($x = 0.15, 0.2$). This change in slope of the electrical conductivity with Nb substitution for Co at high temperatures is explicable by the lattice oxygen loss. This is attributed mainly to the reduction from high valence state Co^{4+} to Co^{3+} , which results in a decrease of the charge carrier concentration.^{2,28} In other words, the suppressed oxygen loss from the lattice with increasing Nb content induce less formation of oxygen vacancies and a consequent decrease in charge carriers, which lowers electrical conductivity. For the perovskite MIECs, transport of oxygen ions and electronic conduction are simultaneously achieved in these oxides. The transport of oxygen ions proceeds through the hopping of oxygen vacancies, while transport of electrons is along the $\text{B}^{n+}-\text{O}^{2-}-\text{B}^{(n-1)+}$ network due to overlapping between B:3d and O:2p orbitals.¹² The increase of Nb doping leads to an increase of non-conducting Nb-O bonds, which obstructs electronic transport through O-Co-O

bonds and, as a result, decreases the electrical conductivity.^{12,16}

Cross-sectional SEM images of a single cell and cathode are displayed in Fig. 8. The bottom side indicates the microstructure of the dense GDC electrolyte and the upper side shows the microstructure of the porous cathode made of LSCNbx/GDC ($x = 0.1$) after calcination at 950 °C, as presented in Fig. 8(a). The thickness of the cathode layer and the GDC electrolyte is approximately 15-20 μm , respectively. The microstructures of all LSCNbx ($x = 0.1, 0.15,$ and 0.2) samples are similar, thus showing that the microstructures of the samples are apparently insensitive to Nb substitution.

The impedance spectra for the symmetric cells (LSCNbx-GDC/GDC/LSCNbx-GDC) by AC impedance spectroscopy with various temperatures in air are shown in Fig. 9. The impedance spectra are fitted to the equivalent circuit. The fitting parameters (R_2 and R_3) are presented as a function of Nb content in the inset of Fig. 9(a). Based on the literature,^{14,29,30} the high and intermediate frequencies behavior of impedance (R_2) is related to ion and electron transfer at the electrode, electrolyte, and collector/electrode interfaces, while the low frequency behavior of impedance, R_3 , is associated with non-charge transfer, such as oxygen surface exchange and gas-phase diffusion inside and outside the electrode layer. From these results, the increase of the R_3 with an increase of Nb content are likely to influence oxygen reduction reaction more than other factors.

Arrhenius plots of the cathode polarization conductance are provided in Fig. 9(b). The non-ohmic resistance values of LSCNbx ($x = 0.1, 0.15,$ and 0.2) symmetrical cells are $0.077 \Omega \text{ cm}^2$, $0.097 \Omega \text{ cm}^2$, and $0.105 \Omega \text{ cm}^2$, respectively at 600 °C. From these data, the apparent activation energies (E_a) of LSCNbx ($x = 0.1, 0.15,$ and 0.2) are calculated to be 107 kJ mol^{-1} , 111 kJ mol^{-1} ,

and 107 kJ mol^{-1} , respectively. The increase of the ASR with an increase of Nb is possibly due to decreased electrical conductivity and oxygen vacancy concentration.^{14,16,31}

The electrochemical impedance spectra of LSCNbx/GDC/Ni-GDC single cell corresponding to the I - V polarization curve through 500 - 650 °C are presented in Fig. 10. In these spectra, the intercepts with the real axis at low frequency designate the total resistance of the cell and the value of high frequency is the ohmic resistance of the cell. The non-ohmic resistance of the cell designating the value between the two intercepts on the real axis determines cell performance associated with oxygen kinetics, such as oxygen diffusion and surface exchange rate. The non-ohmic resistances of the LSCNbx ($x = 0.1, 0.15, \text{ and } 0.2$) are $0.056, 0.062, \text{ and } 0.065 \text{ } \Omega\text{cm}^2$ at 600 °C, respectively.

The performance of the LSCNbx cathodes in SOFCs is measured using the GDC electrolyte with humidified H_2 (3% H_2O) as a fuel and ambient air as an oxidant in a temperature range of 500-650 °C. Figure 11 shows the I - V curves and the corresponding power density of the LSCNbx cathodes. The open-circuit voltages of the LSCNbx cells are typically 0.8 V at 700 °C and increase with decreasing operating temperature. The maximum power densities of the LSCNbx ($x = 0.1, 0.15, \text{ and } 0.2$) cathode material are $1.478, 1.226, \text{ and } 1.156 \text{ W cm}^{-2}$, at 600 °C, respectively. These results are explained by the higher electrical conductivity of the LSCNbx ($x = 0.1$). Therefore, LSCNbx ($x = 0.1$) is the most favourable cathode material candidate, considering its high electrical conductivity and electrochemical performance for IT-SOFC application.

Conclusion

LSCNbx ($x = 0, 0.1, 0.15, \text{ and } 0.2$) perovskite oxides have been investigated as a cathode material for IT-SOFCs. It is observed that Nb doping has a significant effect on the structural

stability, electrical conductivity, and electrochemical performance of the LSCNbx oxides. A fully stable and cubic perovskite structure could be obtained for the LSCNbx oxides with $x \geq 0.1$. LSCNbx ($x = 0.1, 0.15, \text{ and } 0.2$) oxides show gradually decreasing electrical conductivity with increasing Nb doping at the same temperature. The non-ohmic resistance of LSCNbx ($x = 0.1, 0.15, \text{ and } 0.2$) symmetrical cells is $0.077 \Omega \text{ cm}^2$, $0.097 \Omega \text{ cm}^2$, and $0.105 \Omega \text{ cm}^2$, respectively, at $600 \text{ }^\circ\text{C}$. The increase of the ASR with an increase of Nb ($x = 0.1, 0.15, \text{ and } 0.2$), can be explained by the decreased electrical conductivity and oxygen vacancy concentration. The maximum power densities of the single cell are $1.478, 1.226, \text{ and } 1.156 \text{ W cm}^{-2}$, at $600 \text{ }^\circ\text{C}$, respectively, with the LSCNbx ($x = 0.1, 0.15, \text{ and } 0.2$)-GDC composite cathode showing the best performance at $x = 0.1$. From these results, the Nb doped LSCNbx ($x = 0.1$) oxide appears to be a favourable IT-SOFC cathode material, considering its structural stability and electrochemical performance.

Acknowledgements

This research was supported by the Mid-career Researcher Program (2013R1A2A2A04015706), the Basic Science Research Program (2013R1A2A2A01007170, and 2010-0021214) and the BK21 plus (10Z2013001105) funded by the Korea government Ministry of Education through the National Research Foundation of Korea funded by the Ministry of Science, ICT and Future Planning.

References

- 1 A. J. Jacobson, *Chem. Mater.*, 2010, **22**, 660
- 2 K.T. Lee and A. Manthiram, *J. Electrochem. Soc.*, 2006, **153**, A794
- 3 W. Zhou, W. Jin, Z. Zhu and Z. Shao, *Int. J. Hydrogen Energy*, 2010, **35**, 1356
- 4 S. Yang, T. He and Q. He, *J. Alloys Compd.*, 2008, **450**, 400
- 5 W. Zhou, R. Ran and Z. Shao, *J. Power Sources*, 2009, **192**, 231
- 6 H. Fukunaga, M. Koyama, N. Takahashi, C. Wen and K. Yamada, *Solid State Ionics*, 2000, **132**, 279
- 7 L.M. Acuña, J.Peña-Martínez, D. Marrero-López, R.O. Fuentes, P. Nuñez and D.G. Lamas, *J. Power Sources*, 2011, **196**, 9276
- 8 S. Choi, J. Shin and G. Kim. *J. Power Sources*, 2012, **201**, 10
- 9 Z. Shao and S.M. Haile, *Nature*, 2004, **431**, 170
- 10 A.N. Petorv, O.F. Kononchuk, A.V. Andreev, V.A. Cherepanov and P. Kofstad, *Solid State Ionics*, 1995, **80**, 189
- 11 T. Kawada, J. Suzuki, M. Sase, A. kaimai, K. Yashiro and Y. Nigara, *J. Electrochem. Soc.* 2002, **149**, E252
- 12 Z.Q. Deng, J.P. Smit, H.J. Niu, G. Evans, M.R. Li, Z.L. Xu, J.B. Claridge and M.J. Rosseinsky, *Chem. Mater.*, 2009, **21**, 5154
- 13 W. Zhou, W. Jin, Z. Zhu and Z. Shao, *Int. J. Hydrogen Energy*, 2010, **35**, 1356

- 14 S.B. Adler, J.A. Lane and B.C.H. Steele, *J. Electrochem. Soc.*, 1996, **143**, 3554
- 15 H. Kruidhof, H.J.M. Bouwmeester, R.H.E.v. Doorn and A. J. Burggraaf, *Solid State Ionics*, 1996, **63-65**, 816
- 16 Z.Q. Deng, W.S. Yang, W. Liu and C.S. Chen, *J. Solid State Chem.*, 2006, **179**, 362
- 17 W.T.A. Harrison, T.H. Lee, Y.L. Yang, D. P. Scarfe, L.M. Liu and A. J. Jacobson, *Mater. Res. Bull.*, 1995, **30**, 621
- 18 S.J. Lee, P. Muralidharan, S.H. Jo and D.K. Kim, *Electrochem. Commun.*, 2010, **12**, 808
- 19 P.J. Shen, X. Liu, H.H. Wang and W.Z. Ding, *J. Phys. Chem. C*, 2010, **114**, 22338
- 20 T. Nagai, W. Ito and T. Sakon, *Solid State Ionics*, 2007, **177**, 3433
- 21 Z. Yang, C. Yang, C. Jin, M. Han and F. Chen, *Electrochem. Commun.*, 2011, **13**, 882
- 22 A.C. Larson and R.B. von Dreele, General Structural Analysis System (GSAS); Los Alamos National Laboratory: Los Alamos, NM, 1987.
- 23 M. James, T. Tedesco, D.J. Cassidy and R.L. Withers, *Mater. Res. Bull.*, 2005, **40**, 990
- 24 L. Dieterle, D. Bach, R. Schneider, H. Störmer, D. Gerthsen, U. Guntow, E. Ivers-Tiffée, A. Weber, C. Peters and H. Yokokawa, *J. Mater. Sci.*, 2008, **43**, 3135
- 25 A. Weizman, D. Fuks, E.A. Kotomin and D. Gryaznov, *Solid State Ionics*, 2013, **230**, 32
- 26 R.D. Shannon, *Acta Crystallogr. Sect. A*, 1976, **A32**, 751
- 27 F. Wang, Q. Zhou, T. He, G. Li and H. Ding, *J. Power Sources*, 2010, **195**, 3772
- 28 S. Yoo, T.H. Lim, J. Shin, G. Kim, *J. Power Sources*, 2013, **226**, 1.
- 29 S.B. Adler, X.Y. Chen and J.R. Wilson, *J. Catal.*, 2007, **245**, 91
- 30 D. Chen, R. Ran, K. Zhang, J. Wang and Z. Shao, *J. Power Sources*, 2009, **188**, 96

- 31 Q. Li, H. Zhao, L. Huo, L. Sun, X. Cheng and J.-C. Grenier, *Electrochem. Commun.*, 2007, **9**, 1508

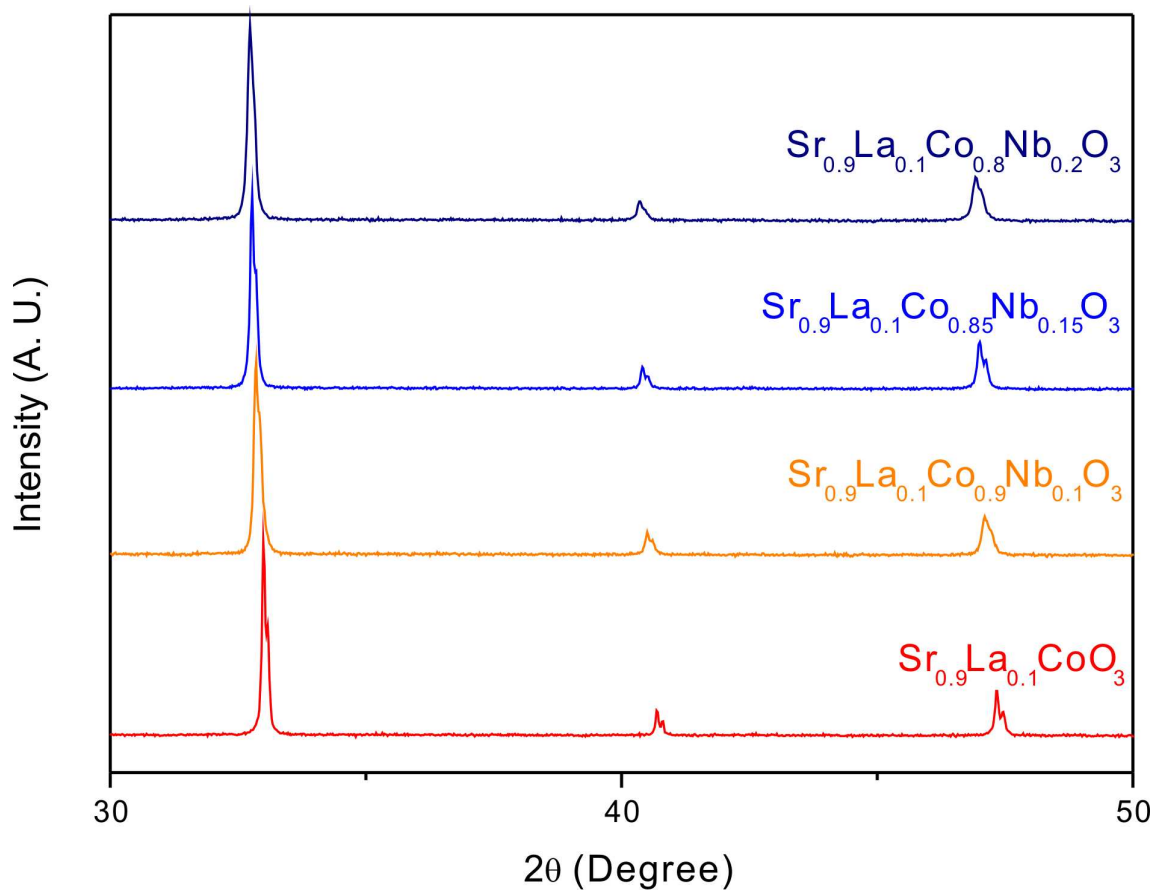


Fig. 1. Powder X-ray diffraction data for $\text{La}_{0.1}\text{Sr}_{0.9}\text{Co}_{1-x}\text{Nb}_x\text{O}_3$ ($x = 0, 0.1, 0.15, \text{ and } 0.2$).

Note that the peak positions shift toward the left-hand side as x increases.

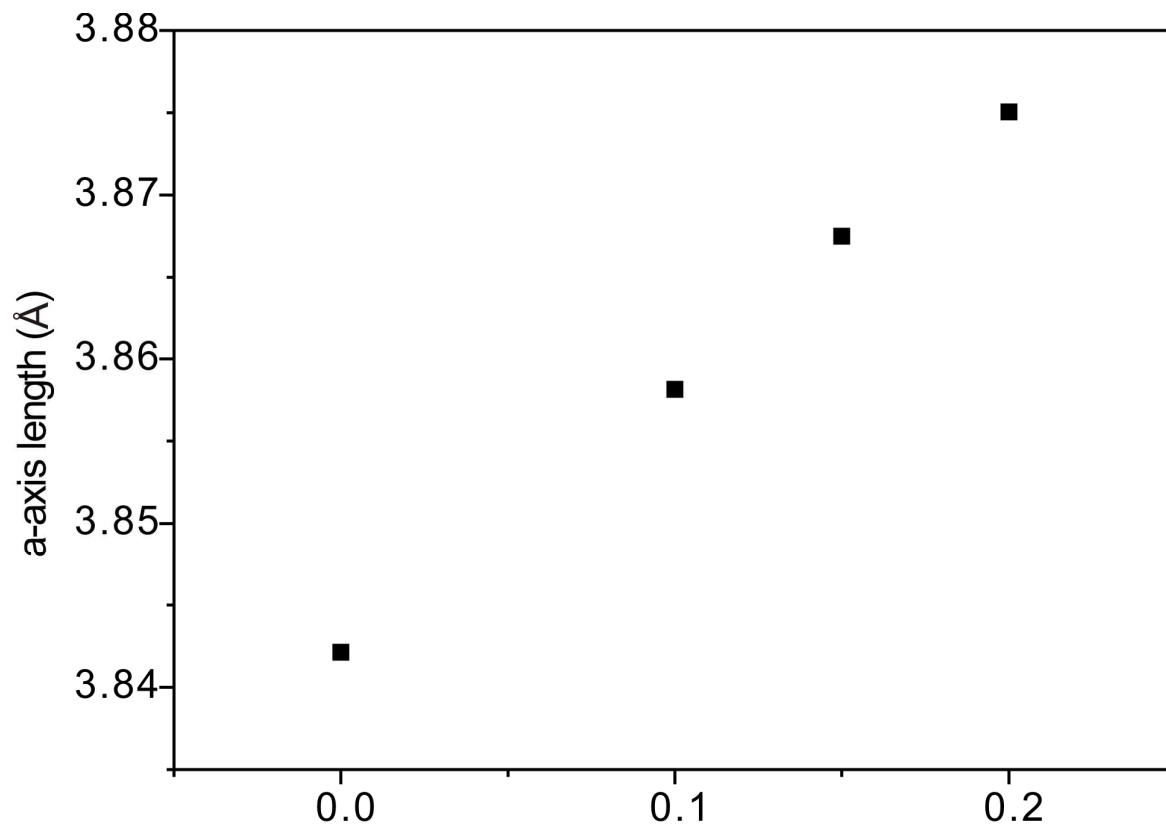


Fig. 2. Variation of the lattice constant (the *a*-axis length) as a function of the Nb content for $\text{La}_{0.1}\text{Sr}_{0.9}\text{Co}_{1-x}\text{Nb}_x\text{O}_3$ solid solutions.

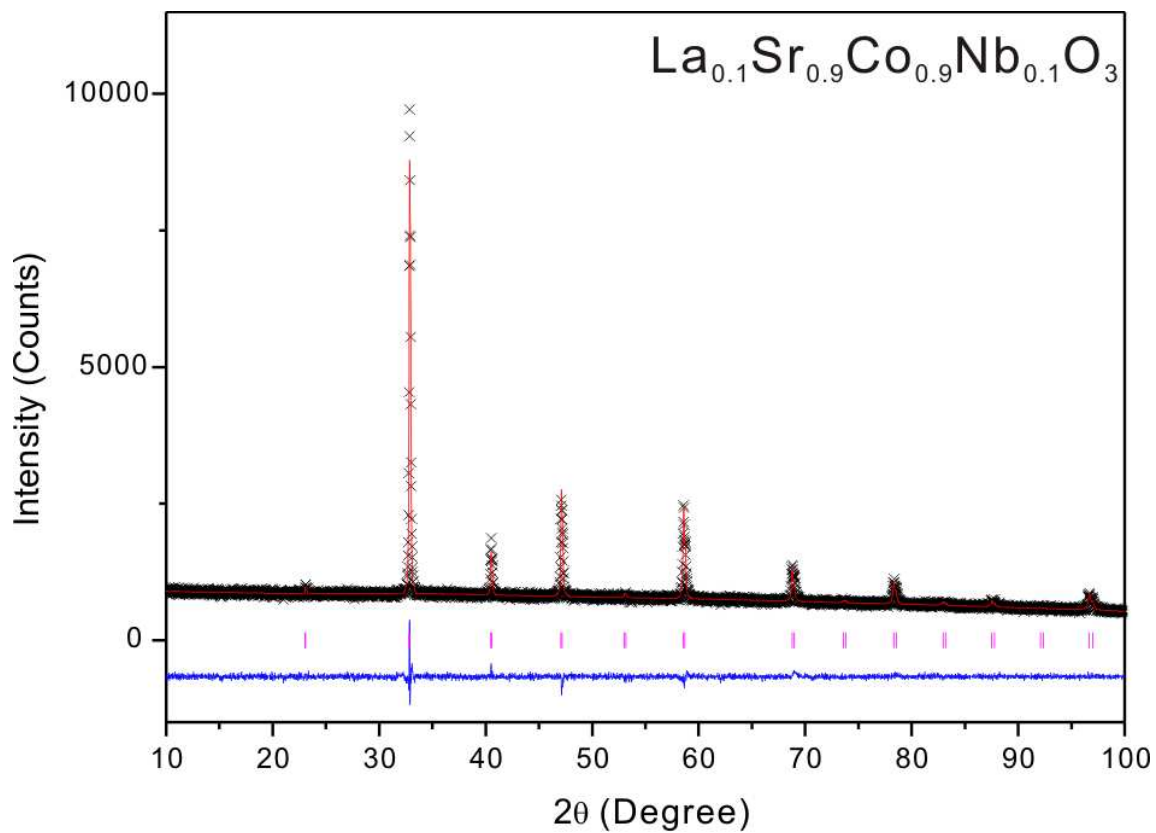


Fig. 3. Final Rietveld plot of an example $\text{La}_{0.1}\text{Sr}_{0.9}\text{Co}_{0.9}\text{Nb}_{0.1}\text{O}_3$. The calculated pattern (red solid line) is compared with observed data (\times). The locations of reflections are indicated by magenta vertical bars. The difference between the observed and calculated profiles is shown at the bottom (blue solid line).

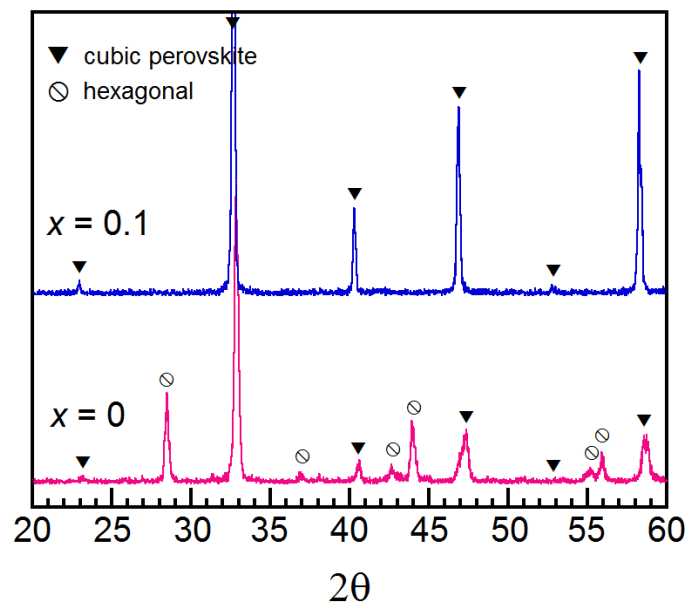


Fig. 4. XRD patterns of $\text{La}_{0.1}\text{Sr}_{0.9}\text{Co}_{1-x}\text{Nb}_x\text{O}_{3-\delta}$ ($x = 0, 0.1$) after annealing at 800°C for 350 h.

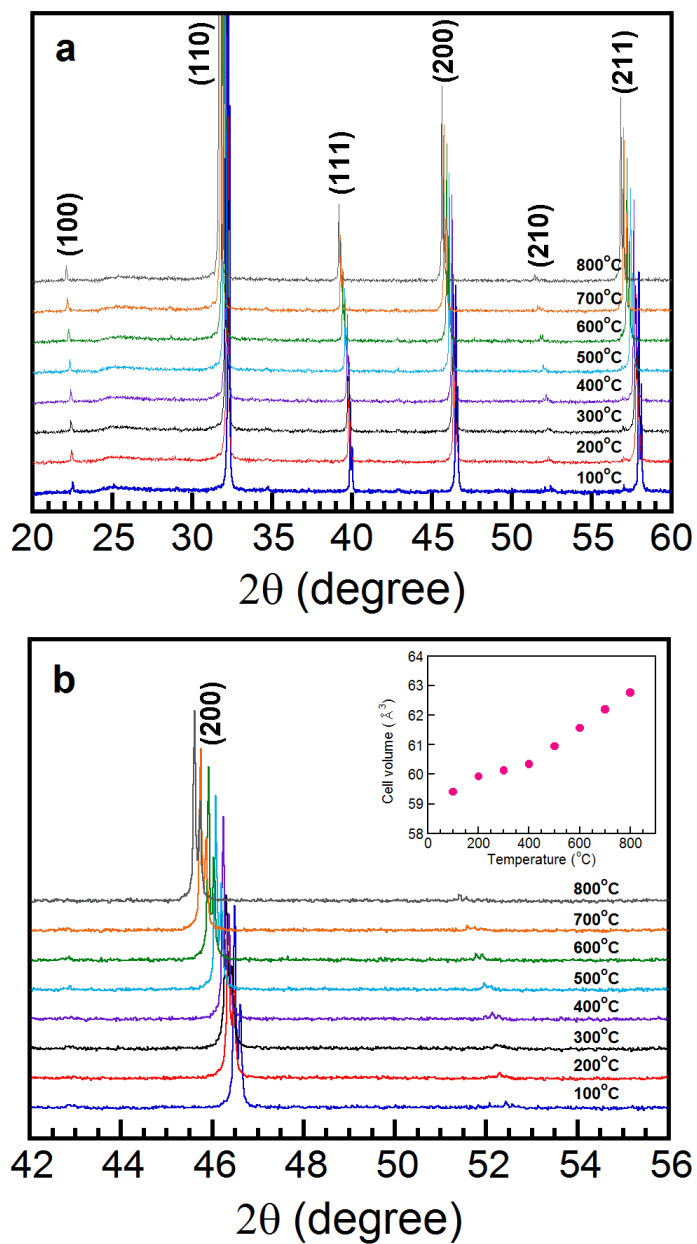


Fig. 5. (a) In-situ XRD patterns of $\text{La}_{0.1}\text{Sr}_{0.9}\text{Co}_{1-x}\text{Nb}_x\text{O}_{3-\delta}$ ($x = 0.1$) at various temperatures, and (b) enlarged in-situ XRD data. The inset shows the effect of temperature on cell volumes (\AA^3).

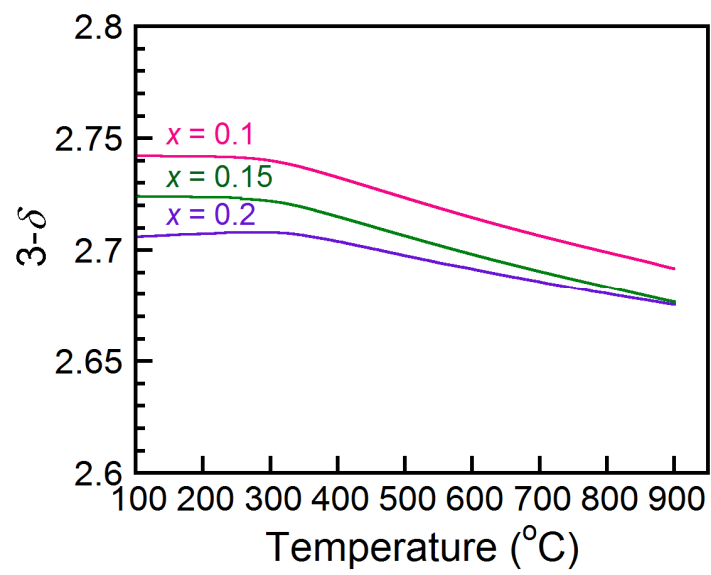


Fig. 6. Thermogravimetric data of $\text{La}_{0.1}\text{Sr}_{0.9}\text{Co}_{1-x}\text{Nb}_x\text{O}_{3-\delta}$ ($x = 0.1, 0.15, \text{ and } 0.2$) as a function of temperature.

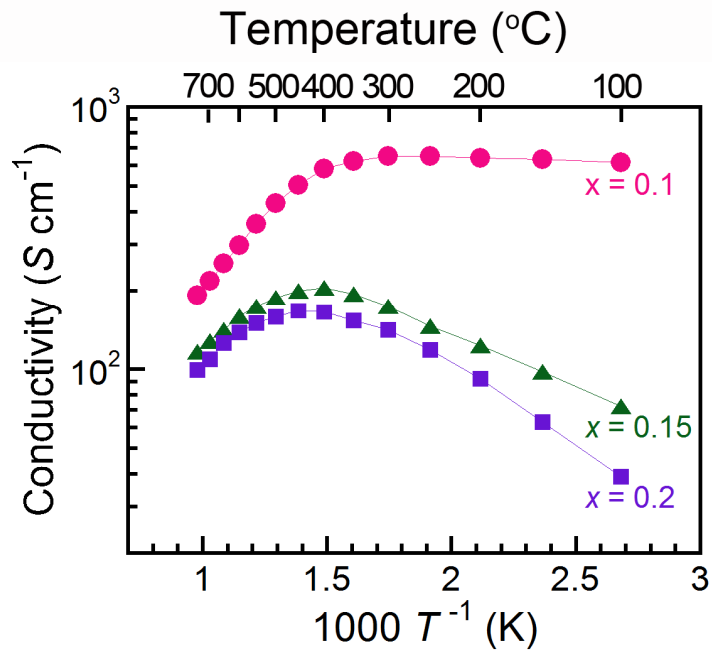


Fig. 7. Electrical conductivities of $\text{La}_{0.1}\text{Sr}_{0.9}\text{Co}_{1-x}\text{Nb}_x\text{O}_{3-\delta}$ ($x = 0.1, 0.15, \text{ and } 0.2$) in air as a function of temperature.

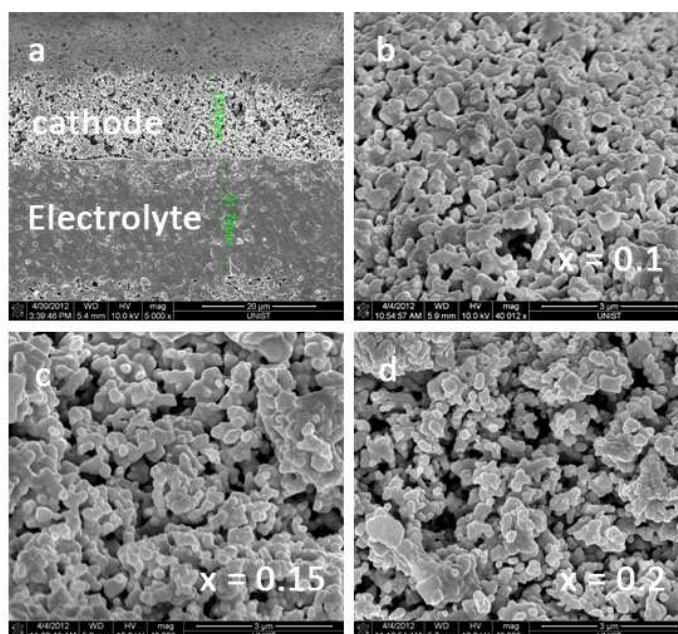


Fig. 8. SEM images of (a) cross-sectional view of the single cell and $\text{La}_{0.1}\text{Sr}_{0.9}\text{Co}_{1-x}\text{Nb}_x\text{O}_{3-\delta}$ cathode with GDC electrolyte in a single cell configuration; (b) $x = 0.1$, (c) $x = 0.15$, and (d) $x = 0.2$.

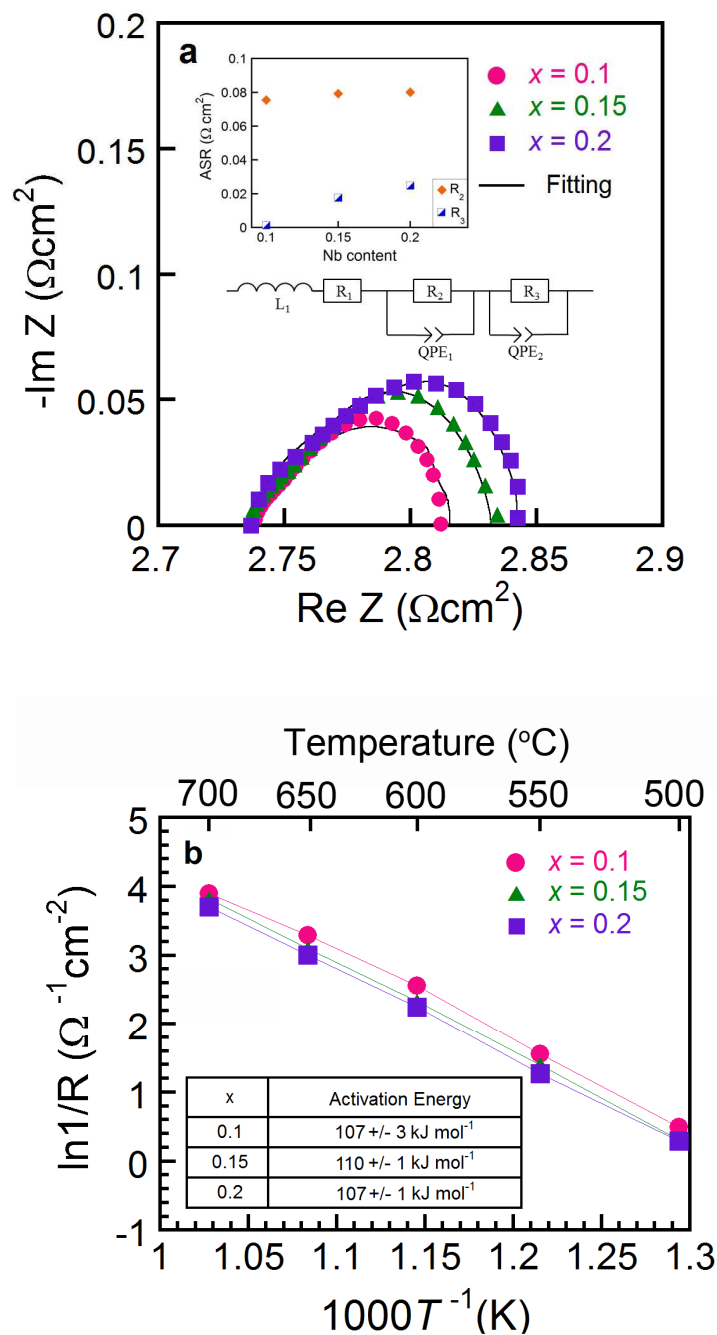


Fig. 9. (a) Impedance spectra and fitted Nyquist plots with $\text{La}_{0.1}\text{Sr}_{0.9}\text{Co}_{1-x}\text{Nb}_x\text{O}_{3-\delta}$ ($x = 0.1$, 0.15 , and 0.2) cathode measured under an open-circuit condition at 600°C in air. (b) Arrhenius plot of the area specific resistance for $\text{La}_{0.1}\text{Sr}_{0.9}\text{Co}_{1-x}\text{Nb}_x\text{O}_{3-\delta}$ ($x = 0.1$, 0.15 , and 0.2) at various temperatures.

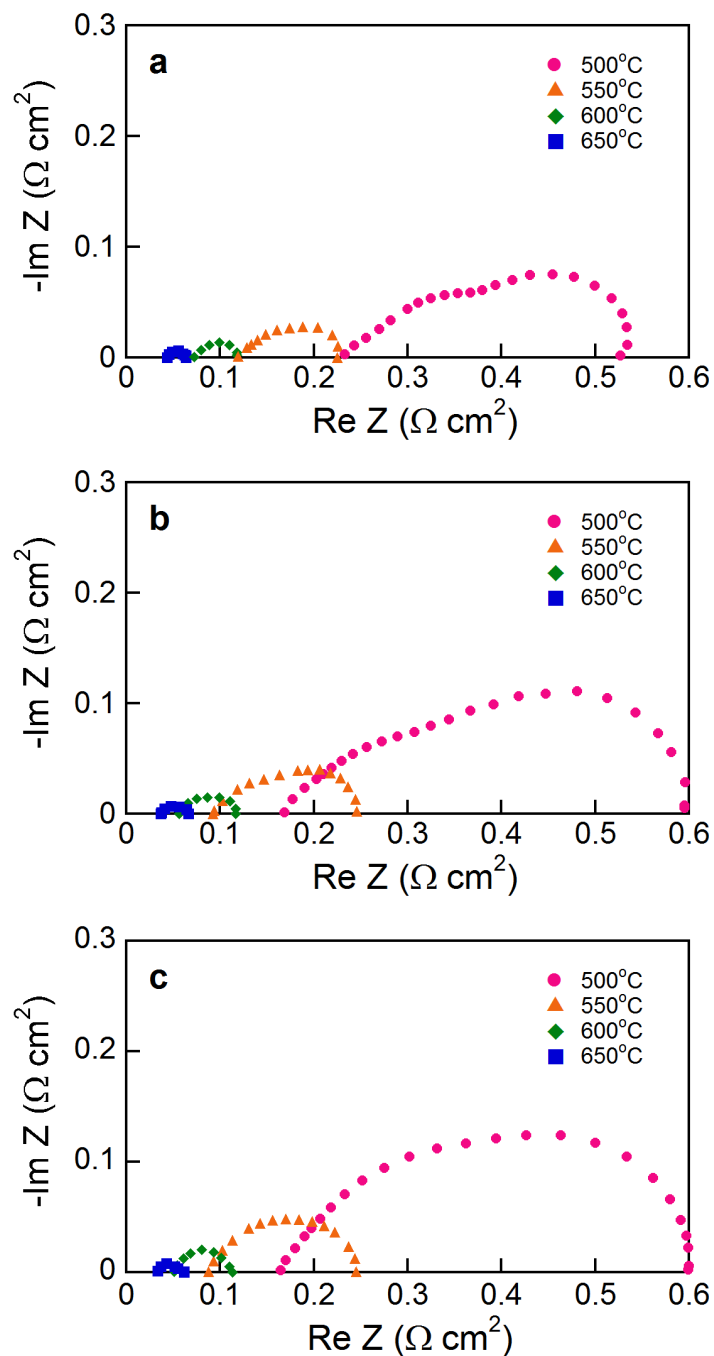


Fig. 10. Impedance spectra of Ni-DC/GDC/ $\text{La}_{0.1}\text{Sr}_{0.9}\text{Co}_{1-x}\text{Nb}_x\text{O}_{3-\delta}$ single cell tested at various temperatures; (a) $x = 0.1$, (b) $x = 0.15$, and (c) $x = 0.2$.

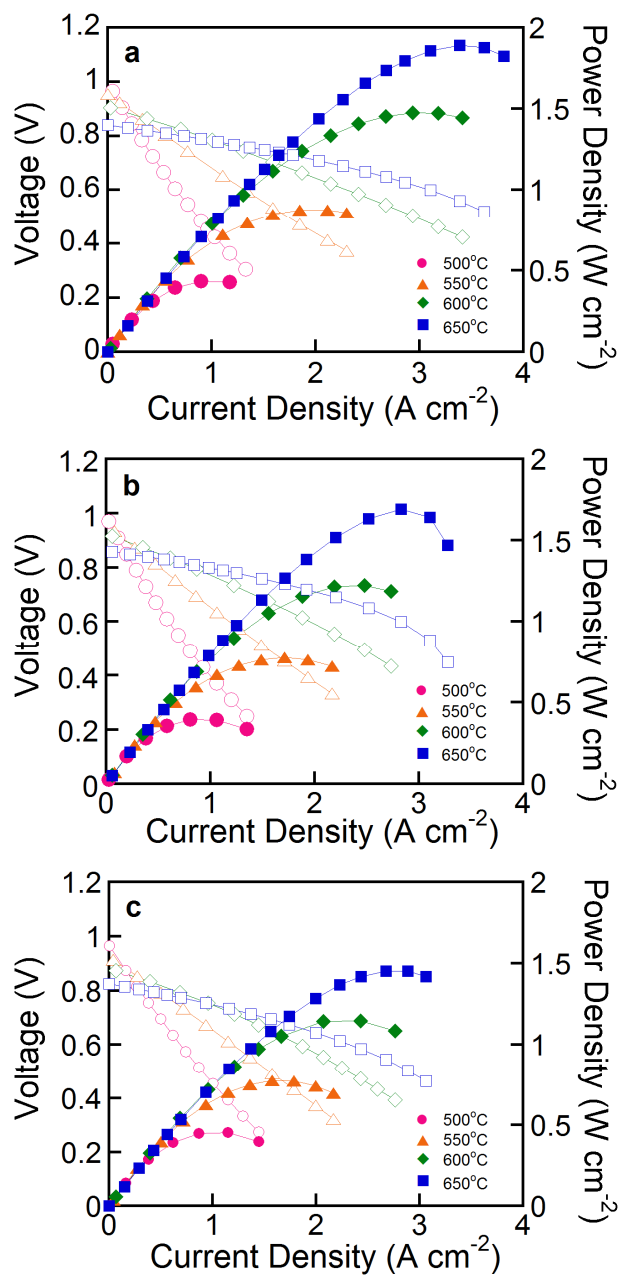


Fig. 11. I - V curves and corresponding power density curves of single cell (Ni-GDC/GDC/ $La_{0.1}Sr_{0.9}Co_{1-x}Nb_xO_{3-\delta}$) at various temperatures; (a) $x = 0.1$, (b) $x = 0.15$, and (c) $x = 0.2$.

Table 1. Summary of Crystallographic Data and Refinement Results for $\text{La}_{0.1}\text{Sr}_{0.9}\text{Co}_{1-x}\text{Nb}_x\text{O}_3$

x	0.0	0.1	0.15	0.2
formula	$\text{La}_{0.1}\text{Sr}_{0.9}\text{CoO}_3$	$\text{La}_{0.1}\text{Sr}_{0.9}\text{Co}_{0.9}\text{Nb}_{0.1}\text{O}_3$	$\text{La}_{0.1}\text{Sr}_{0.9}\text{Co}_{0.85}\text{Nb}_{0.15}\text{O}_3$	$\text{La}_{0.1}\text{Sr}_{0.9}\text{Co}_{0.8}\text{Nb}_{0.2}\text{O}_3$
space group	$Pm-3m$ (No. 221)	$Pm-3m$ (No. 221)	$Pm-3m$ (No. 221)	$Pm-3m$ (No. 221)
$a = b = c$ (Å)	3.842134(19)	3.85814(3)	3.86748(2)	3.87504(3)
V (Å ³)	56.7180(10)	57.4290(10)	57.8470(10)	58.188(2)
λ (Å)	1.5406	1.5406	1.5406	1.5406
R_p^a	0.0292	0.0312	0.0290	0.0307
R_{wp}^b	0.0368	0.0396	0.0368	0.0377

Table 2. Selected Bond Distances (Å) for $\text{La}_{0.1}\text{Sr}_{0.9}\text{Co}_{1-x}\text{Nb}_x\text{O}_3$

$\text{La}_{0.1}\text{Sr}_{0.9}\text{CoO}_3$		$\text{La}_{0.1}\text{Sr}_{0.9}\text{Co}_{0.9}\text{Nb}_{0.1}\text{O}_3$	
Co(1)–O(1) × 6	1.921070(10)	Co(1)/Nb(1)–O(1) × 6	1.92907(2)
Sr(1)/La(1)–O(1) × 12	2.716800(10)	Sr(1)/La(1)–O(1) × 12	2.72811(2)
$\text{La}_{0.1}\text{Sr}_{0.9}\text{Co}_{0.85}\text{Nb}_{0.15}\text{O}_3$		$\text{La}_{0.1}\text{Sr}_{0.9}\text{Co}_{0.8}\text{Nb}_{0.2}\text{O}_3$	
Co(1)/Nb(1)–O(1) × 6	1.933740(10)	Co(1)/Nb(1)–O(1) × 6	1.93752(2)
Sr(1)/La(1)–O(1) × 12	2.73472(2)	Sr(1)/La(1)–O(1) × 12	2.74007(2)